Terahertz magneto-optical properties of bi- and tri-layer graphene

Journal of Physics: Condensed Matter

Terahertz magneto-optical properties of bi- and tri-layer graphene

To cite this article before publication: HongYing Mei *et al* 2018 *J. Phys.: Condens. Matter* in press https://doi.org/10.1088/1361-648X/aab81d

Terahertz magneto-optical properties of bi- and tri-layer graphene

Hongying Mei[1,2], Wen Xu[1,3,*], Chao Wang[1,2], Haifeng Yuan[1,2], Chao Zhang[1], Lan Ding[3], Jin Zhang[3], Chao Deng[4], Yifan Wang[4], Francois M. Peeters[5]

[1]Key Laboratory of Materials Physics, Institute of Solid State Physics, Chinese Academy of Sciences, Hefei 230031, China
[2]University of Science and Technology of China, Hefei 230026, China
[3]Department of Physics and Astronomy, Key Laboratory of Quantum Information of Yunnan Province, Yunnan University, Kunming 650091, China
[4]Daheng New Epoch Technology Inc., Beijing 100085, China
[5]Department of Physics, University of Antwerp, Groenenborgerlaan 171, B-2020 Antwerpen, Belgium

E-mail: wenxu_issp@aliyun.com

November 2017

Abstract. Magneto-optical (MO) properties of bi- and tri-layer graphene are investigated utilizing terahertz time-domain spectroscopy (THz TDS) in the presence of a strong magnetic field at room-temperature. In the Faraday configuration and applying optical polarization measurements, we measure the real and imaginary parts of the longitudinal and transverse MO conductivities of different graphene samples. The obtained experimental data fit very well with the classical MO Drude formula. Thus, we are able to obtain the key sample and material parameters of bi- and tri-layer graphene, such as the electron effective mass, the electronic relaxation time and the electron density. It is found that in high magnetic fields the electronic relaxation time τ for bi- and tri-layer graphene increases with magnetic field B roughly in a form $\tau \sim B^2$. Most importantly, we obtain the electron effective mass for bi- and tri-layer graphene at room-temperature under non-resonant conditions. This work shows how the advanced THz magneto-optical techniques can be applied for the investigation into fundamental physics properties of atomically thin two-dimensional electronic systems.

Submitted to: *J. Phys.: Condens. Matter*

1. Introduction

The basic sample and material parameters of an electronic system, such as the electron density and the electronic relaxation time or mobility, can often be measured via transport and magneto-transport experiments. Over the past decades, terahertz (THz) time-domain spectroscopy (TDS) has become a popular and powerful tool to study the carrier dynamics and optoelectronic properties of different electronic systems [1]. One of the major advantages of the THz TDS technique is that it is a contactless experimental method which enables us to determine directly the real and imaginary parts of the optical conductivity without the need of the Kramers-Kronig transformation [2]. In particular, THz TDS measurements have been intensively applied in recent years for the investigation of the electronic and optoelectronic properties of atomically thin electronic systems and newly developed two-dimensional electron gas (2DEG) systems such as graphene[3–7]. It is known that mono-layer graphene is a massless 2DEG due to its linear-like electronic energy spectrum around the Dirac point [8]. In sharp contrast, electrons in bi- and tri-layer graphene structures have a nonzero effective mass induced mainly by electronic interactions between different carbon layers [9]. Interestingly, it is found that when mono-, bi- and tri-layer graphene are subject to a quantizing magnetic field B, the corresponding Landau level (LL) energy depends on $\sqrt{B}$ for mono-layer graphene [10], on B for bi- and ABA-stacked tri-layer graphene, and on $B^{3/2}$ for ABC-stacked tri-layer graphene [11, 12]. Moreover, the neighboring LL spacing in these graphene structures depends on the LL index [10–12] and, thus, it can differ significantly from the corresponding cyclotron frequency ω_c. As a result, the MO response of electrons in graphene has unique features different from a conventional and semiconductor based 2DEG in which the neighboring LL spacing is simply the cyclotron frequency which does not depend on the LL index. As a matter of fact, these important and interesting features have been examined and demonstrated via low-temperature Fourier MO transmission experiments which measure the MO transition among different LLs in graphene in the infrared (IR) bandwidth [13, 14]. From a viewpoint of physics, the IR Fourier MO absorption or transmission is induced mainly by the inter-LL electronic transition between conduction and valence bands in graphene based structures. In contrast, in THz TDS measurement in the presence of a magnetic field the MO effect is mainly caused by inter- and intra-LL electronic transition events within the same (i.e., conduction or valence band) electronic band in graphene. Therefore, IR Fourier MO measurement and THz MO TDS measurement can measure the consequences of different electronic transition mechanisms.

At present, there has been an intensive experimental investigation of the MO properties of mono-layer graphene and it based electronic devices [13, 15–22]. In particular, it is worth to mention that the IR Fourier MO measurement has been applied to study magneto-plasmonic properties of mono-layer graphene. It has been demonstrated experimentally that the cyclotron resonance and Faraday rotation effects in mono-layer graphene can allow a wide tuning of the working frequency for graphene based plasmonic devices, potentially in the entire THz range, arising from plasmon excitations by the substrate [16] and from different graphene structures such as patterned graphene [17, 18], graphene microribbons [20], graphene metasurface [21]. Moreover, the results obtained from THz and IR MO measurements have shown that mono-layer graphene can serve as a Faraday rotator and non-reciprocal optical isolator in the presence of an external magnetic field [22], predicted theoretically [19]. However, the published experimental results regarding MO properties of bi- and tri-layer graphene are relatively less and the study of the MO properties of graphene has been largely in the IR bandwidth. In this study, we intend examining the basic features of the MO response of bi- and tri-layer graphene in THz regime in the presence of a strong magnetic field. We apply the THz TDS technique in conjunction with high magnetic field condition to achieve this aim. Meanwhile, another prime motivation of this study is to develop a simple and advanced experimental approach to measure optically the key sample and material parameters of these relatively less studied graphene structures.

2. Experimental Techniques

2.1. Sample preparation

The bi- and tri-layer graphene samples used in this study are grown by using the standard chemical vapor deposition (CVD) technique in which the Cu film is applied as catalyst material [23]. After CVD growth of graphene, a thin poly-(methyl methacrylate) (PMMA) film is coated on the graphene/Cu foil. The copper is then etched away by ferric chloride solution and the PMMA/graphene film is placed on quartz substrate by taking the quartz substrate to fish out the PMMA/graphene film in water. The PMMA/graphene/quartz sample is taken for heat treatment, allowing the rough PMMA/graphene film in fully contacting with the quartz substrate. Finally, the PMMA coating layer is removed with acetone. It should be noted that in 0.2 - 1.0 THz regime a graphene/quartz structure is largely transparent to the THz light beams. Such a device structure enables good

transmission of the THz waves through the bi- and tri-layer graphene samples so that the measurement can be undertaken via THz transmission experiments. The samples are with 1×1 cm^2 areal size and the thickness of the quartz substrate is about 1 mm. The Raman and infrared transmission spectra for mono-, bi-, and tri-layer graphene have been employed for the characterization of these samples (see Figures A1 and A2 in Appendix). These results indicate that the bi- and tri-layer graphene samples used in the present study are in high quality both structurally and optically.

2.2. Terahertz time-domain spectroscopy in the presence of magnetic field

In this study, the magneto-optical (MO) measurements are carried out in the standard Faraday configuration, namely both the magnetic field and the incident THz light beam are applied perpendicular to the surface of the graphene films as shown in Figure 1. The details of the experimental setup for the measurement are as follows. i) The femtosecond (fs) fiber laser (ROI optoelectronics, 1.55 μm wavelength, 100 MHz repletion rate, and 80 fs pulse duration) is divided into two beams as pump and probe sources, respectively; ii) The fs pump beam is focused on an InGaAs photoconductive antenna (PCA, Menlo, Germany) to generate a pulsed THz radiation. The corresponding THz spectrum width is from 0.1 to about 2.0 THz; iii) The THz beam is focused on the graphene sample which is placed on the sample holder in a cryostat (ST-500, Janis) with quartz windows. We note here that because the quartz windows are used in the cryostat, which absorb the high frequency THz light, the effective spectrum content of the THz beam focused on the sample is limited within 0.2 THz to about 1.0 THz, in line with previous experimental finding [24]; iv) A superconducting magnet (Cryomagnetics) is applied to tune the strength of the magnetic field from 0 T to 8 T. The direction of the magnetic field is parallel to the propagation direction of the THz beam and perpendicular to the graphene surface; v) The fs probe laser beam is focused on another InGaAs PCA (Menlo, Germany) for the detection of the THz beam transmitted through the graphene sample via the photoconductive sampling; vi) The THz electric field transmitted through the graphene sample is recorded as a function of delay time; vii) Three wire grid polarizers (WGPs) made by polyethylene (TYDEX, Russia) are used to linearly polarize the incident and transmitted THz beams, for the measurement of the THz electric field along different polarization directions. In this measurement setup, the incident THz beam propagates along the z direction and is polarized linearly (by WGP1) along the x direction. WGP2 is applied to polarize the transmitted THz beam with 0°

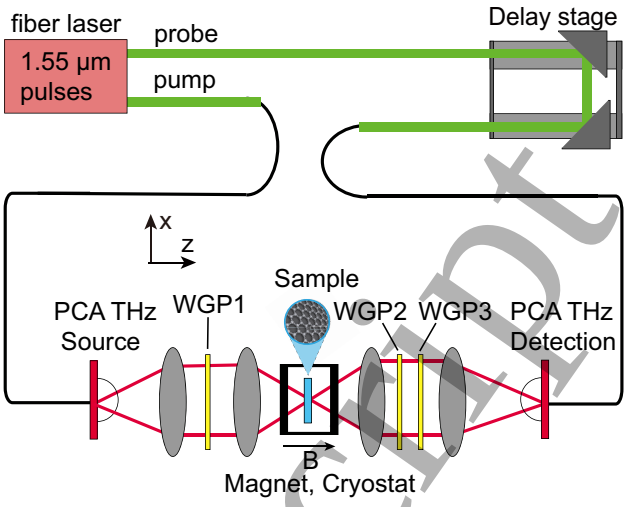

Figure 1. Schematic diagram of the MO THz TDS system. Here WGP is the wire gird polarizer and PCA is the photoconductive antenna.

or ±45° angle to the x direction, for the detection of the polarized light beams by an InGaAs PCA. The system is sealed within a Nitrogen gas environment to reduce the influence of the moisture on measured results. In the present study, the measurements are conducted at room temperature with varying magnetic field from 0 to 8 T and are carried out for both the substrate (quartz) and sample (substrate plus graphene film), respectively.

3. Results

3.1. Terahertz magneto-optical spectrum

The THz TDS measurement of bi- and tri-layer graphene placed on a quartz substrate is conducted in the standard Faraday configuration as shown in Figure 1. The time dependence of the electric field strength of the THz radiation transmitted through the graphene samples is shown in Figure 2 for bi- [in (a), (b) and (c)] and tri-layer [in (d), (e) and (f)] graphene at polarization angles 0° and ±45° and in different magnetic fields as indicated. The obtained data for THz electric field strengths, $E_{+45^\circ}(t)$, $E_{-45^\circ}(t)$, $E_{0^\circ}(t)$, are Fourier transformed to get the corresponding frequency spectrum, $E_{+45^\circ}(\omega)$, $E_{-45^\circ}(\omega)$, $E_{0^\circ}(\omega)$, respectively, which are shown in Figure 3 for bi- [in (a), (b) and (c)] and tri-layer [in (d), (e) and (f)] graphene. As we can see, i) the magnetic field affects mainly the amplitude of $E_\theta(\omega)$ and has a rather weak effect on the phase angle for both bi- and tri-layer graphene samples at different polarization angles; ii) $E_\theta(t)$ and $E_\theta(\omega)$ for bi-layer graphene are larger than those for tri-layer graphene, because a larger THz transmission can be achieved in bi-layer graphene than tri-layer can; iii)

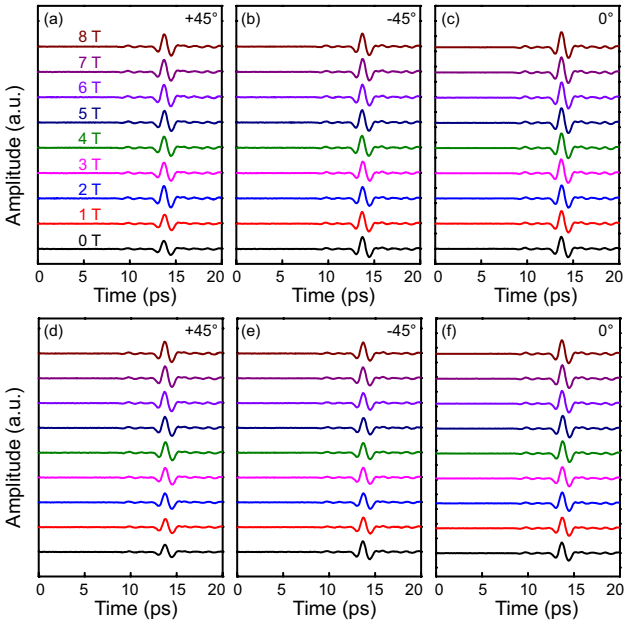

Figure 2. The electric field strength of the THz field transmitted through a graphene sample as a function of delay time for bi- [in (a), (b) and (c)] and tri-layer [in (d), (e) and (f)] graphene at polarization angles 0° and ±45° and in different magnetic fields as indicated.

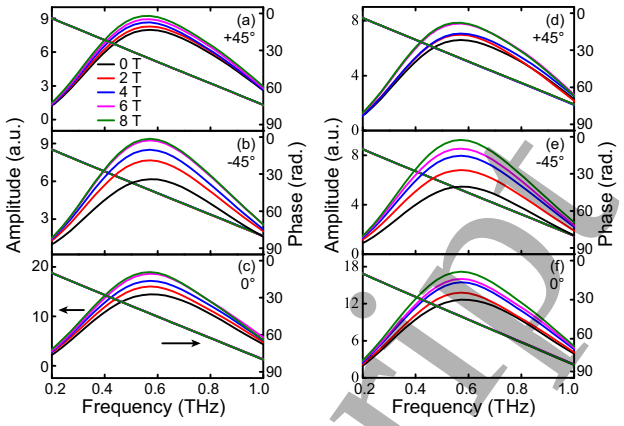

Figure 3. Amplitude and phase angle of the THz field transmitted through bi- [in (a), (b) and (c)] and tri-layer [in (d), (e) and (f)] graphene as a function of radiation frequency $f = \omega/2\pi$ at polarization angles $\theta = 0°$ and $\pm 45°$ and in different magnetic fields as indicated. The results for the phase angles at different B fields coincide.

the amplitude of $E_\theta(t)$ and $E_\theta(\omega)$ increases with the strength of the magnetic field for both bi- and tri-layer graphene samples; and iv) the phase angle of $E_\theta(\omega)$ decreases with THz frequency almost linearly for both bi- and tri-layer graphene. It is slightly larger for tri-layer graphene than that for bi-layer graphene. These results indicate that the magnetic field and the polarized THz radiation can affect the electric field strength of the THz beam transmitted through the sample.

3.2. Magneto-optical conductivities

According to the Fresnel theory, a linearly polarized radiation field can be decomposed into left-handed circularly polarized (LHCP) and right-handed circularly polarized (RHCP) optical modes and there is a difference in the phase shift and amplitude of the transmittance between the LHCP and RHCP modes. Thus, the electric field strengths of the LHCP and RHCP modes can be obtained on the basis of $E_{\pm 45°}(\omega)$ through [25]:

$$\begin{bmatrix} E_l^j(\omega) \\ E_r^j(\omega) \end{bmatrix} = \frac{1}{2}\begin{pmatrix} i-1 & i+1 \\ i+1 & i-1 \end{pmatrix} \times \begin{bmatrix} E_{+45°}^j(\omega) \\ E_{-45°}^j(\omega) \end{bmatrix}, \quad (1)$$

where j represents the result measured for substrate (quartz) or sample (substrate plus graphene film) and $E_l(\omega)$ and $E_r(\omega)$ are respectively the LHCP and RHCP components of the THz field. The faraday ellipticity η and rotation angle θ for a graphene film in the presence of THz and magnetic fields can be calculated, respectively, from

$$\eta(\omega) = \frac{|E_l^{film}(\omega)| - |E_r^{film}(\omega)|}{|E_l^{film}(\omega)| + |E_r^{film}(\omega)|}, \quad (2)$$

and

$$\theta(\omega) = \frac{\arg[E_r^{film}(\omega)] - \arg[E_l^{film}(\omega)]}{2}, \quad (3)$$

with

$$|E_i^{film}(\omega)| = \frac{|E_i^{film+sub}(\omega)|}{|E_i^{sub}(\omega)|}, \quad (4)$$

and

$$\arg[E_i^{film}(\omega)] = \arg[E_i^{film+sub}(\omega)] - \arg[E_i^{sub}(\omega)], \quad (5)$$

where i denotes LHCP or RHCP. For the case of a thin film such as graphene, the complex transverse MO conductivity is given by [26]:

$$\theta(\omega) + i\eta(\omega) \approx \frac{1}{(1+n_{sub})\varepsilon_0 c}\sigma_{xy}(\omega), \quad (6)$$

where $n_{sub} = 1.96$ is the refractive index of the quartz substrate [27], ε_0 is the vacuum permittivity, and $c = 3 \times 10^8$ m/s is the speed of light. Furthermore, the complex longitudinal MO conductivity can be obtained through [28]:

$$\frac{E_x^{film+sub}(\omega)}{E_x^{sub}(\omega)} = \frac{1+n_{sub}}{1+n_{sub}+Z_0\sigma_{xx}(\omega)}, \quad (7)$$

where $E_x(\omega) = E_{0°}(\omega)$ and $Z_0 = 377\ \Omega$ is the impedance of free space. Hence, by combining the THz TDS measurement with MO polarization experiment we are able to obtain the real and imaginary parts of the longitudinal and transverse MO conductivities,

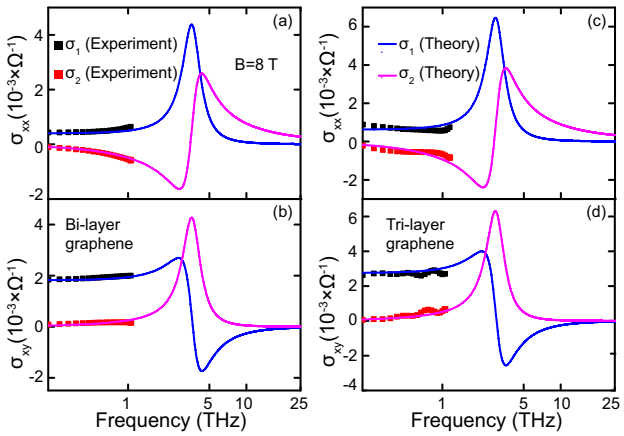

Figure 4. The real (σ_1) and imaginary (σ_2) parts of longitudinal (σ_{xx}) and transverse (σ_{xy}) conductivities for bi- [in (a) and (b)] and tri-layer [in (c) and (d)] graphene as a function of THz radiation frequency $f = \omega/2\pi$ at a fixed magnetic field $B = 8$ T. Here, the dots (curves) are experimental (theoretical) results.

which are four groups of experimental data for each sample.

The real and imaginary parts of the longitudinal $\sigma_{xx}(\omega)$ and the transverse $\sigma_{xy}(\omega)$ MO conductivities for bi- [black and red dots in (a) and (b)] and tri-layer graphene [black and red dots in (c) and (d)] as a function of THz radiation frequency $f = \omega/2\pi$ at a fixed magnetic field $B = 8$ T are shown in Figure 4. We notice that no obvious quantum effect can be observed for the real and imaginary parts of $\sigma_{xx}(\omega)$ and $\sigma_{xy}(\omega)$ for both bi- and tri-layer graphene at $B = 8$ T and at room temperature. Thus, we can employ the classic MO theory to understand and reproduce the experimental findings. It is known that in the THz bandwidth, the MO response of electrons in graphene is mainly achieved mainly via the mechanism of intra-band free carrier optical absorption. Therefore, the classic Drude formula for MO conductivity can be applied to describe the MO properties of bi- and tri-layer graphene, which reads [29]:

$$\sigma_{xx}(\omega) = \frac{\sigma_0(1 - i\omega\tau)}{(1 - i\omega\tau)^2 + (\omega_c\tau)^2},$$
$$\sigma_{xy}(\omega) = \frac{\sigma_0\omega_c\tau}{(1 - i\omega\tau)^2 + (\omega_c\tau)^2}, \quad (8)$$

where $\sigma_0 = n_e e^2\tau/m^*$ is the dc conductivity in the absence of a magnetic field and a light field, n_e is the electron density in the sample, m^* is the electron effective mass, $\omega_c = eB/m^*$ is the cyclotron frequency, τ is the electronic relaxation time, and ω is the radiation frequency. It should be noted that in sharp contrast to the case of massless mono-layer graphene, an electron in bi- and tri-layer graphene can have a nonzero effective mass. In Figure 4, we show and compare the real (σ_1) and imaginary (σ_2) parts of $\sigma_{xx}(\omega)$ and $\sigma_{xy}(\omega)$ for bi- [blue and magenta solid lines in (a) and (b)] and tri-layer graphene [blue and magenta solid lines in (c) and (d)] obtained by THz TDS measurement and by the Drude formula at $B = 8$ T. As one can see, fairly good fitting between experimental and theoretical results can be achieved in the measured THz regime. The peak positions of the blue curves in Figure 4 (a) and Figure 4 (c) correspond to theoretical results where the conditions of the cyclotron resonance are satisfied for bi- and tri-layer graphene, respectively.

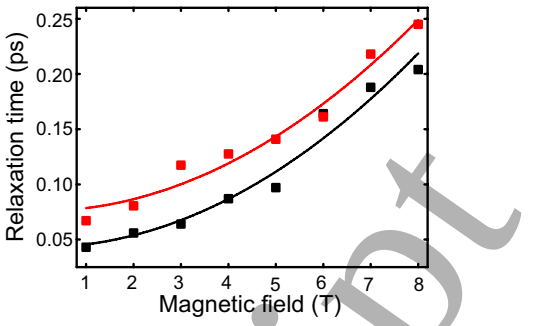

Figure 5. The electronic relaxation time for bi- (black squares) and tri-layer (red squares) graphene as a function of magnetic field. The corresponding curves $\tau = a_0 + a_1 B^2$ are drawn for respectively bi- (black curve) and tri-layer (red curve) graphene.

3.3. Sample and material parameters

By fitting the experimental data with the MO Drude formula, we can obtain the key sample and material parameters such as the electron density n_e, the electron effective mass m^*, and the electronic relaxation time τ for bi- and tri-layer graphene. In doing the fitting, we assume that the electron density in graphene does not alter with varying the magnetic field. As a result, we obtain $n_e = 9.53 \times 10^{16}\ m^{-2}$ and $m^* = 0.063m_e$ for bi-layer graphene along with $n_e = 14.4 \times 10^{16}\ m^{-2}$ and $m^* = 0.077m_e$ for tri-layer graphene, respectively. Here m_e is the rest electron mass. The electronic relaxation time τ as a function of magnetic field for bi- (black squares) and tri- layer (red squares) graphene is shown in Figure 5. We find that τ increases with magnetic field B roughly in a form $\tau = a_0 + a_1 B^2$. Here, $a_0 = 0.04284$ ps and $a_1 = 0.00275$ ps/T^2 for bi-layer graphene (black curve) and $a_0 = 0.07577$ ps and $a_1 = 0.0027$ ps/T^2 for tri- layer (red curve), respectively. It indicates that the tri-layer graphene sample used in this study has a slightly larger electronic mobility than the bi-layer graphene sample does.

4. Discussions

From THz MO TDS measurement conducted at room temperature, we find the electron effective mass (EEM) in bi- and tri-layer graphene to be respectively as $m^* \approx 0.063m_e$ and $0.077m_e$. The electron effective mass in bi- and tri-layer graphene has been a subject for theoretical investigation because it relates closely to the electronic band structure of these graphene systems [30, 31]. The electronic band structure for AB stacked few layer graphene has been calculated on the basis of a tight-binding (TB) approach [30, 31]. It has been found [30] that around the Dirac point, the band EEM for bi-layer graphene is about $0.039m_e$ depending on choosing of the TB parameters. In order to obtain the simple analytical results and to see how the band EEM depends on the band parameters used in the band structure calculation, in this study we evaluate theoretically the band EEM in bi- and tri-layer graphene from simplified electronic band structure in Appendix. Applying a simple effective-mass approximation [32], the EEM for bi-layer graphene around Dirac point in electronic band structure is $m^* = m_0^*/|\cos(3\varphi)|$ depending on the angle φ between electron wavevector $\mathbf{k}$ and the x-axis, which should obviously be larger than $m_0^* = 0.033m_e$. By simple averaging over φ, we find theoretically the band EEM to be $m^* = 0.052m_e$ which is smaller than that obtained from present THz MO TDS experiments. For ABC- and ABA- stacked tri-layer graphene, the electronic band structures are rather complicated. However, it is sure that there is at least one Dirac point at $k = 0$ and the electronic energy spectrum around the Dirac point for tri-layer graphene can be expended as: $E(k, \varphi) = a(\varphi)k^3 + b(\varphi)k^2 + c(\varphi)k + d(\varphi)$. The presence of the k^2 term in the electronic energy spectrum implies that an electron in tri-layer graphene can have a nonzero effective mass. Applying the electronic band structure obtained from the tight-binding calculation for ABC- and ABA-stacked tri-layer graphene [33, 34], we find theoretically that $m^* = 0.14m_e$ for ABC- and $m^* = 0.063m_e$ for ABA-stacked tri-layer graphene. We do not know if the tri-layer graphene sample used in this study is ABC- or ABA-stacked. The value $m^* = 0.077m_e$ obtained from THz MO TDS measurement implies that our sample may have an ABA-stacked structure. We note that the tight-binding model shown in Appendix considers only the nearest-neighbor interaction for ABC-stacked tri-layer graphene and neglects the next nearest-neighbor (NNN) interaction within different carbon layers. The inclusion of the NNN interaction within the calculation can result in a heavier effective mass for an electron in ABA-stacked tri-layer graphene. With increasing carbon layers in graphene structures, the electronic interaction among different carbon layers increases

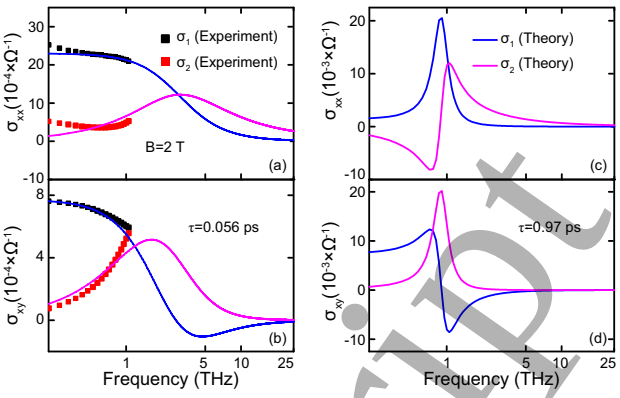

Figure 6. The fitting of the experimental (squares) and theoretical (curves) results for the real (σ_1) and imaginary (σ_2) parts of the longitudinal (σ_{xx}, in (a)) and the transverse (σ_{xy}, in (b)) MO conductivities for bi-layer graphene at $\tau = 0.056$ ps and $B = 2$ T. The theoretical results are shown in (c) and (d) at $B = 2$ T by taking a larger relaxation time $\tau = 0.97$ ps.

and, as a result, the electron can become heavier. This is the main reason why the electron effective mass increases with the number of carbon layers. It should be noted that the band effective mass for an electron in an electronic system may be different from the transport and density-of-state (DoS) effective mass when the electronic energy spectrum is away from a simple parabolic band structure. Generally, the band EEM for graphene can be obtained by taking $k \to 0$ around the Dirac point and by averaging over the band angle. In contrast, the DoS EEM is a consequence after energy averaging over allowed electronic states and the transport EEM is related to an average over electronic states in the presence of electronic scattering centers such as phonons and impurities. The EEM obtained from THz MO TDS measurement corresponds to the transport EEM. Because the electronic energy spectra for bi- and tri-layer graphene are not standard parabolic, it is understandable that the band EEM and the transport EEM in these graphene can be different in values.

At present, the most popularly used experimental method to measure the EEM in an electronic material is through the cyclotron resonance effect (CRE) [35] where a resonant absorption peak can be observed at $\omega \sim \omega_c$ with $\omega_c = eB/m^*$ being the cyclotron frequency induced by the presence of the magnetic field. The condition to be able to observe the measurable CRE is $\omega_c\tau > 1$, which implies that high B field and high mobility sample along with low temperature measurement are required. From theoretical results shown in Figure 4, we notice that ω_c is about 22.3 THz for bi-layer graphene and at 18.1 THz for tri-layer graphene at $B = 8$ T where the CRE can be clearly seen theoretically. However,

such frequencies are beyond the frequency regime of our THz TDS system and, thus, we cannot see the CRE experimentally for bi- and tri-layer graphene at $B = 8$ T at room temperature. In Figure 6(a) and (b) we show the fitting between experimental and theoretical results for real and imaginary parts of $\sigma_{xx}(\omega)$ and $\sigma_{xy}(\omega)$ for bi-layer graphene at $B = 2$ T. The resonant condition $\omega \sim \omega_c$ can be satisfied at $B = 2$ T for our THz MO TDS system. However, the CRE still cannot be seen here both theoretically and experimentally. The reason behind this is that the bi-layer graphene sample has a relatively low mobility or short relaxation time $\tau \approx 0.056$ ps so that the condition $\omega_c\tau > 1$ cannot be satisfied at $B = 2$ T. If we increase the relaxation time to $\tau = 0.97$ ps, the CRE can be clearly seen theoretically using the MO Drude formula, as shown in Fig. 6 (c) and (d). Therefore, high mobility graphene samples are required in order to observe directly the CRE via THz MO TDS measurement at room temperature.

It should be noted that the MO Drude formula is derived within a relaxation time approximation, in which the dependence of the electronic relaxation time τ on magnetic field is not considered. In low magnetic fields, τ often does not vary markedly with B. However, in high B fields τ should be a function of the magnetic field. From the present THz MO TDS measurements, we find that τ increases with B^2 via roughly a dependence of $\tau = a_0 + a_1B^2$ for both bi- and tri-layer graphene. We notice that the THz MO TDS experiments measure directly the MO conductivities. In high magnetic fields, the real part of the Hall conductivity σ_{xy} is much larger than that of the longitudinal conductivity (see Figure 4 for both bi- and tri-layer graphene at $B = 8$ T). Thus, the DC MO resistivity $\rho_{xx} \approx \sigma_{xx}\rho_{xy}^2 \sim \tau B^2$ increases monotonously with magnetic field. Furthermore, in the presence of high magnetic field, the strong cyclotron movement of electrons in graphene can result in an electronic localization effect [36] so that the strength of the effective interaction between electrons and scattering centers such as impurities and phonons can be reduced. As a result, the electronic relaxation time increases with B in high B fields, as shown in Fig. 5 for bi- and tri-layer graphene.

We note that the bi- and tri-layer graphene samples used in this study are produced by the standard CVD growth on Cu catalytic films. The CVD grown graphene normally cannot achieve a high carrier mobility at room temperature due to defects induced during high temperature CVD growth and to basically the polycrystalline natures of the graphene film. Furthermore, the graphene layer is placed on quartz substrate which can provide, e.g., phonon scattering to electrons in graphene at room temperature. As a result, the CVD grown graphene is not as perfect as that of exfoliated graphene and the effects such as defects induced during sample growth, polycrystalline structure, and phonon scattering from substrate can result in relatively low carrier mobility [37]. These are the main reasons why electronic mobility of our samples are lower than those obtained from mechanical exfoliation.

5. Summary

In this study we have developed an experimental technique, on the basis of magneto-optical (MO) THz time-domain spectroscopy, to measure the real and imaginary parts of the longitudinal (σ_{xx}) and transverse (σ_{xy}) MO conductivities for bi- and tri-layer graphene placed on a quartz substrate in the presence of a strong magnetic field. Through fitting of the experimental data with the classical MO Drude formula, we obtained optically the key sample and material parameters for these graphene structures, such as the electron density, the electron effective mass, and the electronic relaxation time. We have examined the dependence of the electronic relaxation time in bi- and tri-layer graphene upon the strength of the magnetic field and found that τ increases with B^2. Most significantly, we have obtained the electron effective mass (EEM) for bi- and tri-layer graphene at room temperature under non-resonant conditions. It has been found that the EEM in tri-layer graphene is larger than that in bi-layer graphene. The EEMs obtained from THz MO TDS measurements for bi- and tri-layer graphene are slightly larger than those from theoretical evaluation on the basis of band structure calculation. These experimental findings clearly demonstrate that the THz MO TDS technique is a powerful and convenient tool for the investigation and characterization of 2D electronic systems such as few-layer graphene. We hope the results obtained from this work can help one to gain an in-depth understanding of the magneto-optical properties of graphene.

Acknowledgement

This work was supported by the National Science Foundation of China (11574319, 11304317, 11304272), the Ministry of Science and Technology of China (2011YQ130018), the Center of Science and Technology of Hefei Academy of Science, the Department of Science and Technology of Yunnan Province, and by the Chinese Academy of Sciences.

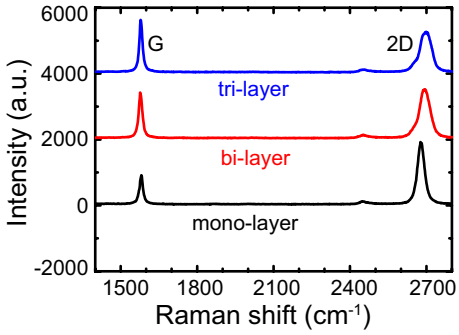

Figure A1. The Raman spectra for mono-, bi- and tri-layer graphene grown on quartz substrates and used in the current study. The result for mono-layer graphene is shown for comparison.

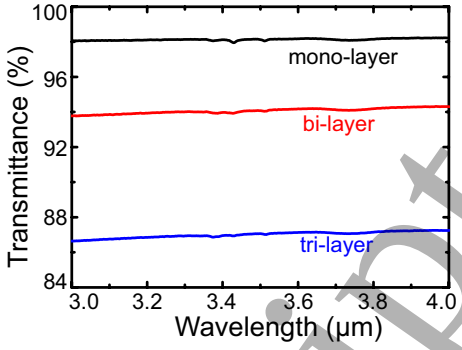

Figure A2. The infrared transmittance of mono-, bi- and tri-layer graphene samples used in the current study. The result for mono-layer graphene is shown for comparison.

Appendix A. Sample characterization

Raman spectroscopy is commonly used to determine the number of carbon layers in graphene [38]. In the present study, an excitation laser with a wavelength of 514 nm and a focused spot size of 1 μm in diameter is applied to measure the Raman spectra for mono-, bi- and tri-layer graphene. The spectral resolution of the system is 8 cm^{-1} (obtained with a 600 grooves/mm grating) in the Raman spectroscopy setup. The corresponding Raman spectra are shown in Figure A1, there are two prominent peaks: the G band at about 1580 cm^{-1} and the 2D band at about 2700 cm^{-1}. The peak position and line shape of the G band reflect the sample doping and the 2D band is mainly related to its electronic structure [39, 40]. From Figure *A1*, we calculate the I_{2D}/I_G ratio and the results are 2.1, 1.07 and 0.78, in consistent with mono-, bi- and tri-layer, respectively [41–43]. Moreover, we can also observe the blue-shifts of the 2D peaks in Raman spectra with increasing number of the carbon layers in graphene.

In order to characterize the optical properties of the graphene samples used in this study, we conducted the infrared transmission measurements. A Si carbide rod is employed as a broadband infrared incident light source. The spectrum is recorded using Bruker 66v Fourier transform infrared (FTIR) spectrometer where the DTGS detector is used for the detection in the 3-4 μm wavelength regime. By definition, the transmittance for graphene is the square ratio of the sample (graphene and quartz substrate) and substrate (quartz). The transmittance is 98.1%, 94.2%, 87.1% for mono-, bi- and tri-layer graphene respectively in this light bandwidth. These results are slightly smaller than the transmittances observed in the visible bandwidth for mono-, bi- and tri-layer graphene [41]. The results obtained from Raman and infrared measurements indicate that the bi- and tri-layer graphene samples used in this study are of good quality.

Appendix B. Theoretical analysis of the electron effective mass for bi- and tri-layer graphene

Here we evaluate the band effective mass for an electron in bi- and tri-layer graphene on the basis of the simplified theoretical models.

Bi-layer graphene

Under the effective-mass approximation, the electronic energy spectrum for bi-layer graphene around the Dirac point can be written as [32]:

$$E_\lambda(k) = \lambda \frac{\hbar^2 k K}{2m_0^*}, \tag{B.1}$$

where $\lambda = \pm 1$ for conduction or valence band, $m_0^* \approx 0.033 m_e$, $K = \sqrt{k^2 + k_0^2 - 2kk_0\cos(3\varphi)}$ with $k_0 \approx 5.77\times10^5$ cm^{-1}, and φ is the angle between k and the x-direction. It is known that there are four Dirac points for bi-layer graphene. One is at $k\to0$ and the other three are at $\varphi=0$, $2\pi/3$ and $4\pi/3$ when $k\to k_0$. When $k\to0$, we have

$$E_\lambda(k) \approx \frac{\lambda\hbar^2}{2m_0^*}\left[k_0 k - k^2\cos(3\varphi) + \frac{k^3}{2k_0}\sin^2(3\varphi)\right]. \tag{B.2}$$

The band electron effective mass around $k\to0$ is determined by

$$\frac{1}{m^*} = \frac{1}{\hbar^2}\frac{\partial^2 E_\lambda(k)}{\partial k^2} = \frac{|\cos(3\varphi)|}{m_0^*}, \tag{B.3}$$

depending on the angle φ and m^* obviously being larger than m_0^*. After simple averaging over φ, the electron effective mass for bi-layer graphene is obtained via

$$\overline{M^*} = m_0^*\left[\frac{1}{2\pi}\int_0^{2\pi}|\cos(3\varphi)|d\varphi\right]^{-1} \approx 0.052 m_e. \tag{B.4}$$

When $k \to k_0$, after expanding the energy spectrum around $k \to k_0$ we get

$$E_\lambda(k) \approx \frac{\lambda\hbar^2}{2m_0^*}\left[\sqrt{2(1-\cos(3\varphi))}k_0 k + \sqrt{\frac{1-\cos(3\varphi)}{2}}(k-k_0)k\right] + o(k-k_0)^2. \quad \text{(B.5)}$$

The corresponding band electron effective mass at $k \to k_0$ is

$$\frac{1}{m^*} = \frac{1}{\hbar^2}\frac{\partial^2 E_\lambda(k)}{\partial k^2} = \frac{\sin^2(3\varphi/2)}{m_0^*}. \quad \text{(B.6)}$$

Because the corresponding Dirac points are at φ=0, $2\pi/3$ and $4\pi/3$, an electron is massless around these Dirac points, similar to the case of mono-layer graphene. As a result, the electron effective mass in bi-layer graphene is mainly induced by the electronic band structure around k=0 and should be larger than $0.033m_e$. The theoretical value for the band EEM in bi-layer graphene, after a simple angle averaging, is found to be $0.052m_e$.

Trilayer graphene

ABC-stacked tri-layer graphene. The electronic energy spectrum obtained from the tight-binding model for ABC-stacked tri-layer graphene is given as [33]:

$$E_\lambda(k) = h_s + \lambda\sqrt{h_c^2 + h_t^2 + 2\cos(3\varphi)h_c h_t}, \quad \text{(B.7)}$$

where $\lambda = \pm 1$ for conduction or valence band, $h_s = \delta - 3\gamma_0\gamma_4(ka)^2/2\gamma_1$, $h_c = (\sqrt{3}\gamma_0 ka)^3/8\gamma_1^2$, $h_t = \gamma_2/2 - 3\gamma_0\gamma_3(ka)^2/(2\gamma_1)$. Here $\gamma_0, \gamma_1, \gamma_2, \gamma_3, \gamma_4$ are the Slonczewski-Weiss-McClure (SWM) hopping parameters obtained by fitting the band structures from density functional theory (DFT) [44] in ABC-stacked tri-layer graphene.

When $k \to 0$, there is a Dirac point and the band EEM is

$$\frac{1}{m^*} = \frac{1}{\hbar^2}\frac{\partial^2 E}{\partial k^2} = -\frac{3\gamma_0 a^2(\gamma_3+\gamma_4)}{\hbar^2\gamma_1}. \quad \text{(B.8)}$$

When taking [33] $\gamma_0 = 3.16$ eV, $\gamma_1 = 0.502$ eV, $\gamma_2 = -0.0171$ eV, $\gamma_3 = -0.377$ eV and $\gamma_4 = -0.099$ eV, the band electron effective mass for ABC-stacked tri-layer graphene is $m^* = 0.14m_e$.

ABA-stacked tri-layer graphene. The energy spectrum obtained from the tight-binding model for ABA-stacked tri-layer graphene is composed of six energy bands given by [34]:

$$E_{\pm 1} = \pm\frac{\hbar^2 K^2}{2m_1},$$
$$E_{\pm 2} = \pm\hbar v_f^{'} K,$$
$$E_{\pm 3} = \pm\left(\frac{\hbar^2 K^2}{2m_3} + \triangle\right). \quad \text{(B.9)}$$

Here $m_1 = m_3 = t_1/(\sqrt{2}v_f^2)$, $v_f = 3t_0 a_0/(2\hbar)$, a_0 is the lattice vectors, t_0 refers to the in-plane hopping, and t_1 relates to inter-plane hopping. If we consider $E_{\pm 1} = \pm\hbar^2 K^2/(2m_1)$ around the Dirac points ($K_\pm$ points), the band electron effective mass is obtained as

$$m^* = m_1 = t_1/(\sqrt{2}v_f^2) = \frac{4\hbar^2 t_1}{9\sqrt{2}t_0^2 a_0^2}. \quad \text{(B.10)}$$

After taking the band parameters [34] as $t_0 = 2.7$ eV, $t_1 = 0.4$ eV, and $a_0 = 0.142$ nm, the band electron effective mass for ABA-stacked tri-layer graphene is obtained as $0.063m_e$.

[1] Ulbricht R, Hendry E, Shan J, Heinz T F and Bonn M 2011 *Rev. Mod. Phys.* **83** 543–586
[2] Lloyd-Hughes J and Jeon T I 2012 *J. Infrared, Millimeter, Terahertz Waves* **33** 871–925
[3] Lee C, Kim J Y, Bae S, Kim K S, Hong B and Choi E J 2011 *Appl. Phys. Lett.* **98** 071905
[4] Lee S H, Choi M, Kim T T, Lee S, Liu M, Yin X, Choi H, Lee S S, Choi C G, Choi S Y, Zhang X and Min B 2012 *Nat. Mater.* **11** 936–941
[5] George P A, Strait J, Dawlaty J, Shivaraman S, Chandrashekhar M, Rana F and Spencer M G 2008 *Nano Lett.* **8** 4248–4251
[6] Docherty C J and Johnston M B 2012 *J. Infrared, Millimeter, Terahertz Waves* **33** 797–815
[7] Docherty C J, Lin C T, Joyce H J, Nicholas R J, Herz L M, Li L J and Johnston M B 2012 *Nat. Commun.* **3** 1228
[8] Orlita M and Potemski M 2010 *Semicond. Sci. Technol.* **25** 063001
[9] Yin L J, Li S Y, Qiao J B, Nie J C and He L 2015 *Phys. Rev. B* **91** 115405
[10] Jiang Z, Henriksen E A, Tung L C, Wang Y J, Schwartz M E, Han M Y, Kim P and Stormer H L 2007 *Phys. Rev. Lett.* **98** 197403
[11] Yin L J, Bai K K, Wang W X, Li S Y, Zhang Y and He L 2017 *Front. Phys.* **12** 127208
[12] Yuan S, Roldán R and Katsnelson M I 2011 *Phys. Rev. B* **84** 125455
[13] Gusynin V P, Sharapov S G and Carbotte J P 2006 *J. Phys.: Condens. Matter* **19** 026222
[14] Crassee I, Levallois Walter A L, Ostler M, Bostwick A, Rotenberg E, Seyller T, van der Marel D and Kuzmenko A B 2011 *Nat. Phys.* **7** 48–51
[15] Shimano R, Yumoto G, Yoo J Y, Matsunaga R, Tanabe S, Hibino H, Morimoto T and Aoki H 2013 *Nat. Commun.* **4** 1841
[16] Crassee I, Orlita M, Potemski M, Walter A L, Ostler M, Seyller T, Gaponenko I, Chen J and Kuzmenko A B 2012 *Nano Lett.* **12** 2470–2474
[17] Yan H, Li Z, Li X, Zhu W, Avouris P and Xia F 2012 *Nano Lett.* **12** 3766–3771
[18] Poumirol J M, Liu P Q, Slipchenko T M, Nikitin A Y, Martin-Moreno L, Faist J and Kuzmenko A B 2017 *Nat. Commun.* **8** 14626
[19] Lin X, Wang Z, Gao F, Zhang B and Chen H 2014 *Sci. Rep.* **4** 4190
[20] Tymchenko M, Nikitin A Y and Martin-Moreno L 2013 *ACS Nano* **7** 9780–9787
[21] Hadad Y, Davoyan A R, Engheta N and Steinberg B Z 2014 *ACS Photonics* **1** 1068–1073
[22] Tamagnone M, Moldovan C, Poumirol J M, Kuzmenko A B, Ionescu A M and Mosig J R 2016 *Nat. Commun.* **7** 11216
[23] Suk J W, Kitt A, Magnuson C W, Hao Y F, Ahmed S, An J, Swan A K, Goldberg B B and Ruoff R S 2011 *ACS Nano* **5** 6916–6924

[24] Hangyo M, Nagashima T and Nashima S 2002 *Meas. Sci. Technol.* **13** 1727–1738
[25] Morikawa O, Quema A, Nashima S, Sumikura H, Nagashima T and Hangyo M 2006 *J. Appl. Phys.* **100** 033105
[26] Ikebe Y, Morimoto T, Masutomi R, Okamoto T, Aoki H and Shimano R 2010 *Phys. Rev. Lett.* **104** 256802
[27] Parker T J, Ford J E and Chambers W G 1978 *Infrared Phys.* **18** 215–219
[28] Tinkham M 1956 *Phys. Rev.* **104** 845–846
[29] Han F W, Xu W, Li L L and Zhang C 2016 *J. Appl. Phys.* **119** 245706
[30] Partoens B and Peeters F M 2006 *Phys. Rev. B* **74** 075404
[31] Partoens B and Peeters F M 2007 *Phys. Rev. B* **75** 193402
[32] Dong H M, Zhang J, Peeters F M and Xu W 2009 *J. Appl. Phys.* **106** 043103
[33] Xiao Y M, Xu W, Zhang Y Y and Peeters F M 2013 *Phys. Status Solodi B* **250** 86–94
[34] Rashidian Z, Bludov Y V, Ribeiro R M, Peres N M and Vasilevskiy M I 2014 *J. Phys.: Condens. Matter* **26** 395301
[35] Spitzer W G and Fan H Y 1957 *Phys. Rev.* **106** 882–890
[36] Aoki H and Ando T 1981 *Solid State Commun.* **38** 1079–1082
[37] Liu W, Li H, Xu C, Khatami Y and Banerjee K 2011 *Carbon* **49** 4122–4130
[38] Ferrari A C and Basko D M 2013 *Nat. Nanotechnol.* **8** 235–246
[39] Lui C H, Li Z, Chen Z, Klimov P V, Brus L E and Heinz T F 2010 *Nano Lett.* **11** 164–169
[40] Hao Y, Wang Y, Wang L, Ni Z, Wang Z, Wang R, Koo C K, Shen Z and Thong J T L 2010 *Small* **6** 195–200
[41] Sun Z, Raji A R O, Zhu Y, Xiang C, Yan Z, Kittrell C, Samuel E L G and Tour J M 2012 *ACS Nano* **6** 9790–9796
[42] Tung V C, Allen M J, Yang Y and Kaner R B 2009 *Nat. Nanotechnol.* **4** 25–29
[43] Tongay S, Lemaitre M, Miao X, Gila B, Appleton B R and Hebard A F 2012 *Phys. Rev. X* **2** 011002
[44] Zhang F, Sahu B, Min H and MacDonald A H 2010 *Phys. Rev. B* **82** 035409